测绘出版社 SURVEYING AND MAPPING PRESS

SAR Azimuth Cut-off to Estimate Wind Speed under High Wind Regimes

Valeria CORCIONE[1], Ferdinando NUNZIATA[1], Marcos PORTABELLA[2], Giuseppe GRIECO[3], Xiaofeng YANG[4], Maurizio MIGLIACCIO[1]

1. *Università degli Studi di Napoli Parthenope*, *Dipartimento di Ingegneria*, *Naples* 80133, *Italy*; 2. *The institute of Marine Sciences* (*ICM-CSIC*), *Barcelona* 08003, *Spain*; 3. *Koninklijk Nederlands Meterologisch Instituut* (*KNMI*), *De Bilt* 3731, *The Netherlands*; 4. *State Key Laboratory of Remote Sensing Science*, *Aerospace Information Research Institute*, *Chinese Academy of Sciences*, *Beijing* 100101, *China*

Abstract: In this study, the azimuth cut-off method, typically used for SAR moderate wind speed estimation purposes, is analyzed under high wind regimes. Firstly, the importance of the pixel spacing, the size of the boxes selected for Synthetic Aperture Radar (SAR) image partitioning and the image texture in terms of homogeneities are discussed by considering their influence on the azimuth cut-off (λc) estimation. Secondly, a quality control analysis of the reliability of λc is carried out by evaluating the distance between the autocorrelation functions (ACF) and their correspondent fittings. This analysis points out the importance of filtering out the unreliable and unfeasible λc values in order to improve the wind speed estimation. The quality control procedure is based on a x^2 test, applied on a large Sentinel-1A dataset. The soundness of the test is verified by an increment in terms of correlation between λc estimations and wind speed values. This approach is, then, applied under high wind regimes, i.e., tropical cyclones.

Key words: SAR; wind speed; azimuth cut-off; significant wave height

Citation: Valeria CORCIONE, Ferdiinando NUNZIATA, Marcos PORTABELLA, et al. SAR Azimuth Cut-off to Estimate Wind Speed under High Wind Regimes[J]. Journal of Geodesy and Geoinformation Science, 2021, 4(1): 30-37. DOI: 10.11947/j.JGGS.2021.0104.

Wind speed is one among the key variables driving oceanic and atmospheric processes. It is possible to obtain accurate information about sea surface thanks to satellite microwave active sensors, which has a well-known fundamental role in this context. In particular, scatterometers are typically used for wind field estimation and they are able to obtain a 25-km resolution product[1]. Because of the coarse resolution of these sensors, recently, the Synthetic Aperture Radar (SAR) gained great interest in wind speed estimation. In fact, SAR sensors can reach resolutions of the order of few meters[2-5].

The most common approach to retrieve wind field is based on the Normalized Radar Cross Section (NRCS) or radar backscatter. Several empirical Geophysical Model Functions (GMFs), originally developed to exploit C-band VV-polarized scatterometer measurements[6-7], have been tuned and recalibrated to deal with SAR measurements. However, the radar backscatter is sensitive to both wind speed and wind direction. Then, a priori knowledge of the wind direction is needed to retrieve wind speed[8]. The so-called azimuth cut-off technique, originally proposed by in Literature [9] to derive sea surface wind speed, does not need neither calibration of the data nor any a priori information on wind direction[10].

The theoretical basis for the azimuth cut-off method is related to the influence of the orbital motion of the surface waves in the SAR imaging of the ocean surface. This orbital motion results in additional Doppler shifts that distort the phase of the backscattered signal that is used to synthetize the resolution in azimuth. The result is a low-pass filtered SAR image in the azimuth direction[11]. The

Received date: 2020-10-10; accepted date: 2020-12-25

First author: Valeria CORCIONE (1989—), female, post-doctoral student, majors in electromagnetic modeling, SAR data analysis, and ocean remote sensing.

E-mail: valeria.corcione@uniparthenope.it

azimuth cut-off well correlates to the SWH because of its sensitivity to the long waves. Within this context, a brief review of some relevant works is carried out. In Literature[9] the ERS 1-2 SAR dataset is analyzed to discuss the azimuth cut-off in terms of Significant Wave Height (SWH) and wind speed; while, in Literature[12] the Sentinel-1 dataset acquired under moderate and high wind regimes (up to 25 m/s) is used for wind speed retrieval, adopting the azimuth cut-off approach. In particular, a linear model is adopted only under fully developed sea state conditions.

Recently, there is a growing interest in accurately measure sea surface parameters under very high wind conditions, such as in Tropical Cyclones (TCs)[13-18]. In this work, the azimuth cut-off approach is revised and adapted to such wind conditions. A new optimized way to evaluate the SAR azimuth cut-off is also proposed.

1 Methodology

This study wants to find a robust criterion leading to an accurate estimation of λc, independently from any wind regimes. In particular, the azimuth cut-off approach is reviewed in terms of the pixel spacing and box sizes. The azimuth cut-off (λc) can be estimated as follows[12]:

① The SAR image is divided into SAR imagette of 10 km×10 km.

② The autocorrelation function (ACF) of each imagette is evaluated by applying an inverse fast Fourier transformation (IFFT) of the Power Spectral Density (PSD).

③ A 70 mmedian filter window is applied.

④ The Gaussian function that best fits the obtained truncated ACF is retrieved.

⑤ The λc estimate is linked to the standard deviation of the obtained Gaussian fit.

When dealing with surface and estimation, typically StripMap SAR imagery is used and, therefore, the shown methodology is specialized using the following parameters: SAR imagery is subdivided into blocks of area 10×10 km^2 and a 7-pixels median filter is applied[12] (that is equivalent to 70 mfor an image of 10 mazimuth resolution). This rationale is typically used to deal with low-to-moderate wind regimes. When dealing with extreme wind conditions cases a twofold problem should be addressed: on one side, SAR observation of tropical cyclones claims for a large area coverage that at once, suggests choosing the ScanSAR acquisition mode. On the other side, inhomogeneities due to high variability at the microwave reflectivity are in place. This means that azimuth cut-off procedure must be re-tuned taking into account these two issues: the ScanSAR mode (which results in a spatial resolution different than the StripMap one) and inhomogeneities. In detail, it is independent on the SAR spatial resolution; secondly, to analyze block size in order to minimize inhomogeneities related to rain effects and attenuation bands. To make clearer the above-mentioned issues, a meaningful test case is shown, that is based on a TerraSAR-X (TS-X) ScanSAR mode image collected on October 21, 2010 with a spatial resolution of 8.25 m. To clearly point out the two dependencies of λc estimation from the box size and the azimuth resolution, a tailored analysis is presented that consists of exploiting the SAR scene to evaluate λc using different box sizes and by gradually downgrading the azimuth resolution. Results are depicted in Fig.1 where two spatial resolutions are considered (i.e. 8 m, 33 m, see Fig.1 (a) (i)—(b) (i), respectively) and, for each spatial resolution, the λc estimation is undertaken considering 2 block sizes, i.e. 2 km and 4 km, see Fig.1 (a)(ii) and (b)(ii).

Experimental results clearly point out that both the spatial resolution and block size play a key role in the estimation of λc. In addition, it can be also noted that λc estimation is critical when undertaken within inhomogeneities related to attenuation bands. In detail, spatial resolution significantly affects λc estimation with coarser spatial resolutions resulting in the worst estimation. In addition, the longer is the box size, the poorer is the estimation since the areas affected by the inhomogeneity gets longer and longer. However, it can be also noted that all this matter arises when dealing with the inhomogeneity. In fact,

λc is well-estimated over areas that do not exhibit inhomogeneities almost independently of spatial resolution and box size.

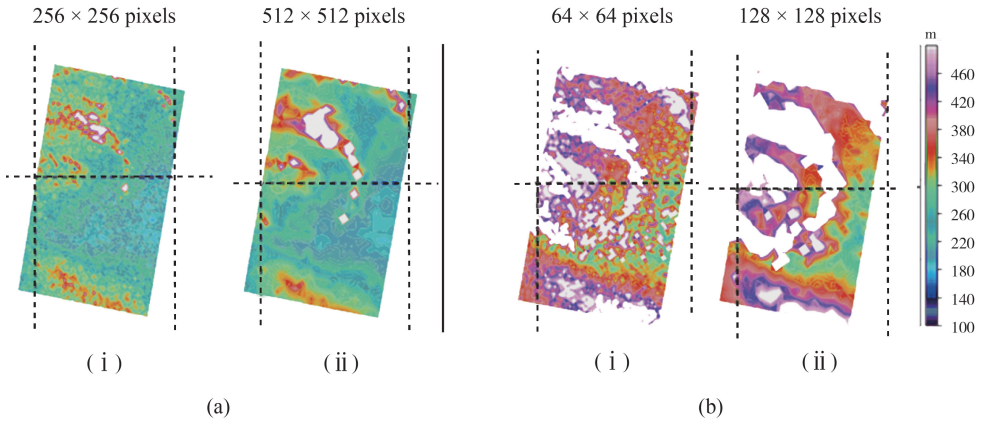

Fig.1 Estimation of λc using the TS-X SAR imagery and considering different pixel spacings (8 m (a), 33 m (b)), and different box sizes (2 km (i) and 5 km (ii))

2 Sensitivity Analysis of Pixel Spacing and Box Size

In this section, λc estimation is discussed with respect to pixel spacing and box size to achieve a robust criterion that allows wind retrieval when inhomogeneities are in place, e. g., under extreme weather condition cases. First, a sensitivity analysis of λc estimation with respect to pixel spacing is carried out. In Fig. 2 λc estimations obtained using a median filter and fitting the actual ACF (continuous line) with a Gaussian bell (dashed line) are shown. Note that results refer to the estimation undertaken over a homogeneous area and different pixel spacings are considered downgrading the nominal spatial resolution (8 m) up to 132 m. In Fig.2 (a) the conventional 11-pixel median filter is adopted to estimate λc. The estimated values confirm the results obtained in Fig.1 and, hence, exhibit a significant dependence on the spatial resolution. In fact, λc estimates referred to the same area increase when the pixel spacing gets coarser. This is an unwanted artifact that is inherently related to the estimation process. To investigate this drawback, instead of the conventional 11-pixel median filter, a variable-size median filter whose window's size adapted to the pixel spacing is used. Experimental evidence suggests using a median filter whose window's size is within the range 90~120 m. In detail, when dealing with 8 m pixel spacing, the best window's size, i.e., the window's size that results in the most reliable λc estimate is 11—13 pixels; while when dealing with 17 m the window's size should be set at 8—9 pixels; for 33 m pixel spacing a window's size of 3 ~ 5 m is needed. This corresponds to set window's sizes ranging from 1 pixel to 11 pixels. This implies that, when the pixel spacing is coarser than 50 m, λc estimation is no longer reliable since the median filter has no effect. λc estimates are shown in Fig.2 (b) show that in this case more reliable estimates are obtained. In fact, λc does not change significantly when the pixel spacing changes. Note that, estimates that result from pixel spacings coarser than 50 m are not listed.

With regard to the box size, the analysis aims at selecting the minimum box size that results in reliable λc estimates for a given median filter window. Hence, a homogeneous area is considered in the SAR scene and nested boxes whose sizes vary in the range 64×64—4096×4096, i.e., in the range 0.6~41 km. This analysis is undertaken on a C-band Sentinel-1 SAR scene collected on March 6, 2015 in the East Atlantic area. Note that TS-X SAR scene of the previous experiment cannot be used here, since it is not enough homogeneous. Experimental results are shown in Fig.2 (c) where the actual ACF (continu-

ous line) and the Gaussian fit (dashed line) are shown. The different colours refer to the different box sizes. It can be noted that all the curves exhibit tails with the exception of the 64×64 one (see continuous and dashed blue lines) which does not exhibit tails since there are not enough points at 10 m pixel spacing. It can be noted that λc values do not change significantly with respect to the box size. Hence, one can select the smallest box size in order to minimize the effects related to inhomogeneities in SAR imagery. In this case, the smallest box size is the 128×128 pixels one since the 64×64 pixels does not ensure a good number of points to reliably estimate λc.

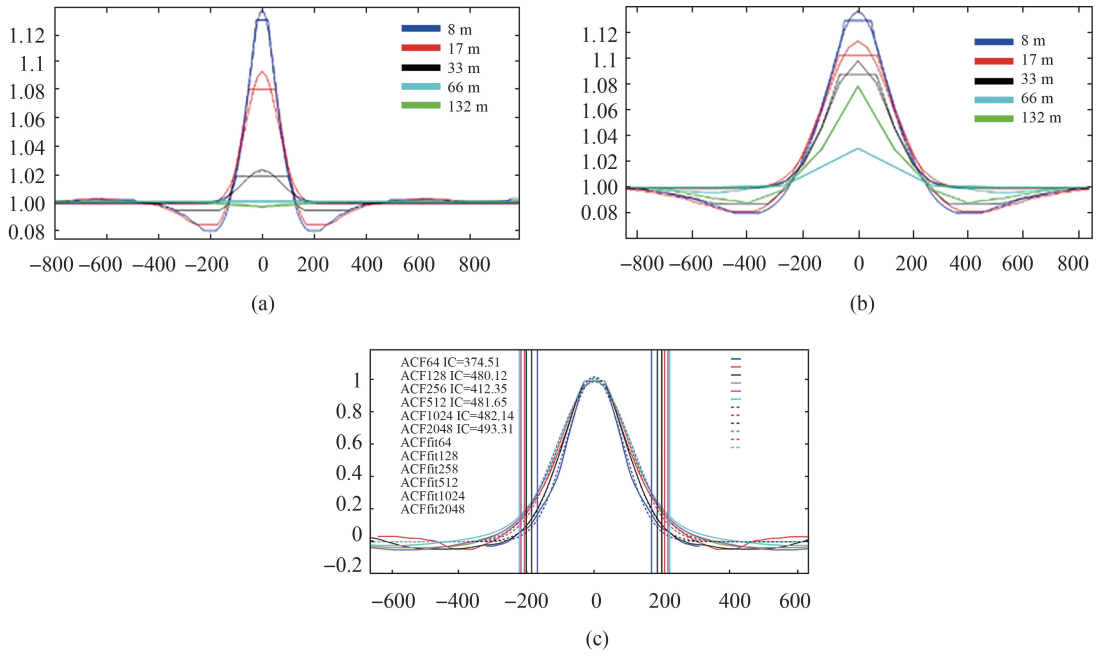

Fig.2 ACF (continuous line) and its Gaussian fit (dashed line) obtained using a 11-pixel median filter (a) and variable window's size median filter (b) for pixel spacings equal to 8 m, 17 m, 33 m, 66 m and 132 m (different colours). (c) ACF (continuous line) and the Gaussian fit (dashed line) are estimated over a SAR VV StripMap Sentinel-1 homogeneous area using a 11-pixels median filter applied over nested boxes whose size range from 64×64 pixels to 2048×2048 pixels (see different colours)

3 Quality Analysis

In this section, a misfit analysis is carried out in order to evaluate the reliability of the proposed method. The quality control (QC) consists of first computing, the difference between the ACF and its Gaussian fit (see, e.g., the difference between the red solid and the red dotted curves in Fig.2) in the half main lobe of the function. More in detail, a x^2 test is conducted for each box.

The test is conducted over 355 Sentinel-1 images in StripMap mode with 10 m pixel spacing. Interpolated European Centre for Medium-Range Weather Forecasts (ECMWF) wind speed output to the SAR acquisition time and location is used to verify the effectiveness of the x^2-based filter. Note that the QC-passed 1-km λc estimates are averaged into a 10-km λc estimate, which is then compared against the auxiliary SWH data.

Several x^2-based thresholds have been tested and 0.06 found to be the most effective. Note that also unfeasible λc values higher than 700 m are filtered out since they are unfeasible values. Fig. 3 shows that the correlation between λc and wind speed increases from Literature[12] when using the proposed x^2-based QC with a threshold of 0.06. This is a clear indication that the proposed QC method is indeed effective.

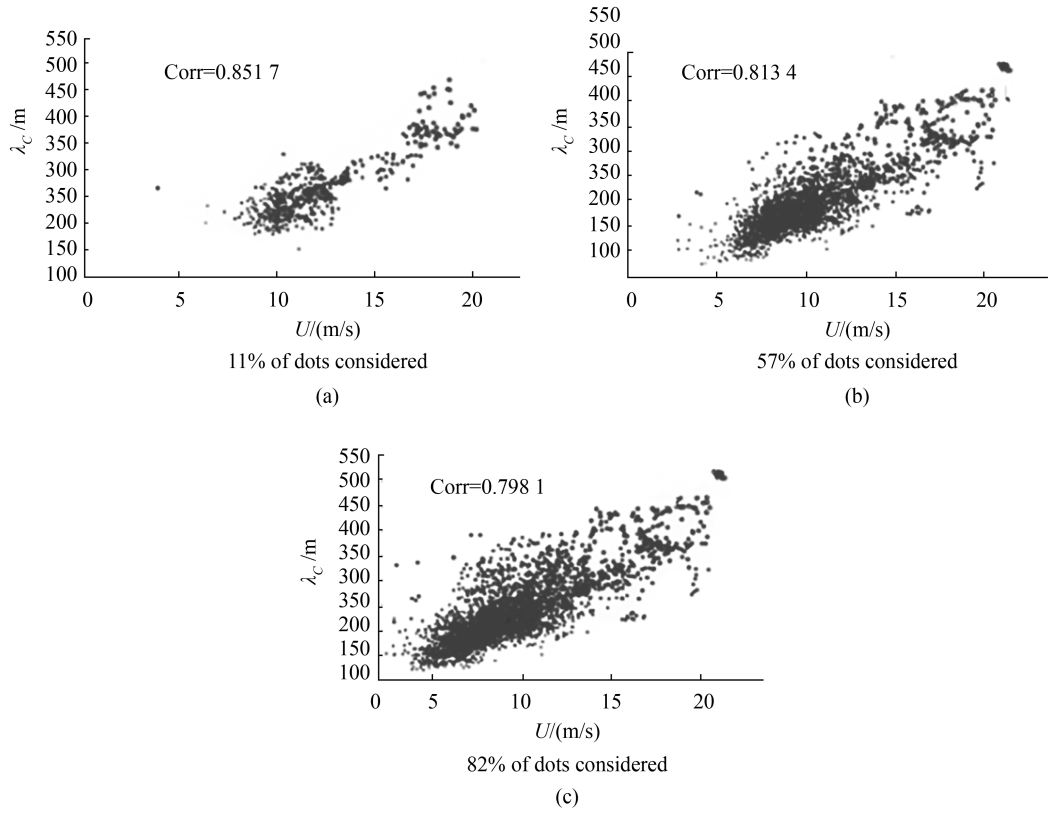

Fig.3 Wind speed retrieved using azimuth cut-off under different sea age conditions. (Scatterplots between U and λc refer to analysis undertaken using $th=0.1$ (a), $th=1$ (b) and $th=3$ (c), respectively.)

To compare azimuth cut-off values with the ECMWF one, fully developed sea state conditions must be verified. On this purpose, Pierson-Moskowitz (PM) criterion is adopted in Literature [19]. Hence, the azimuth cut-off is evaluated on the data points which satisfy the following criterion

$$|SWH-SWHFD| < th \quad (1)$$

Where SWHFD is the SWH for a fully developed sea state and th is a threshold. In Fig.11, th is set to 0.1. Fig.3 (a) depicts the scatterplot between sea surface wind speed (U) and λc. It can be noted that when $th=0.1$, only 11% of the total data points satisfy Eq.(1). Hence, only 11% of the data points call for fully-developed sea state conditions that result in a good correlation coefficient (>0.85). When relaxing the threshold (Fig.3 (b) and (c)) the correlation is still good (around 80%). This is a strong result, saying that the linear model can be still adopted when conditions far from the fully developed sea state are taking place.

4 Tropical Cyclone Case

In this section, the novel azimuth cut-off approach, proposed in this study, is applied under extreme weather conditions, i.e., tropical cyclones. The considered dataset is a Sentinel-1A Interferometric Wide (IW) mode collected on September 1, 2016, in occasion of Hurricane Hermine.

In Fig.4 (a) the wind speed map provided by Ifremer is shown. This map is compared with the azimuth cut-off map obtained by taking into account the criteria described in this study. The concentration of the higher winds seems to be respected in the second map, and this result is verified by the scatterplots depicted in Fig.5 (a) and (b).

In particular, two scatterplots have been analyzed, one for the northern region of the map shown in Fig.4, and one for the southern one, see Fig.5. The two plots show that the correlation between the retrieved λc is very good (higher than 90%) for the southern region, see Fig.5 (b); while, the correla-

tion hardly exceeds 57% percentage for the southern region, see Fig.5 (b). This result is not surprising, since the northern region of the map includes a more critical area, that includes the hurricane center and more frequent rain patterns, and, consequently, more inhomogeneities. But, in a region far enough from the center, the azimuth cut-off approach seems to work well. The reasoning of this result could be found by exploiting a well known sea state parameter, the inverse wave age, Ω.

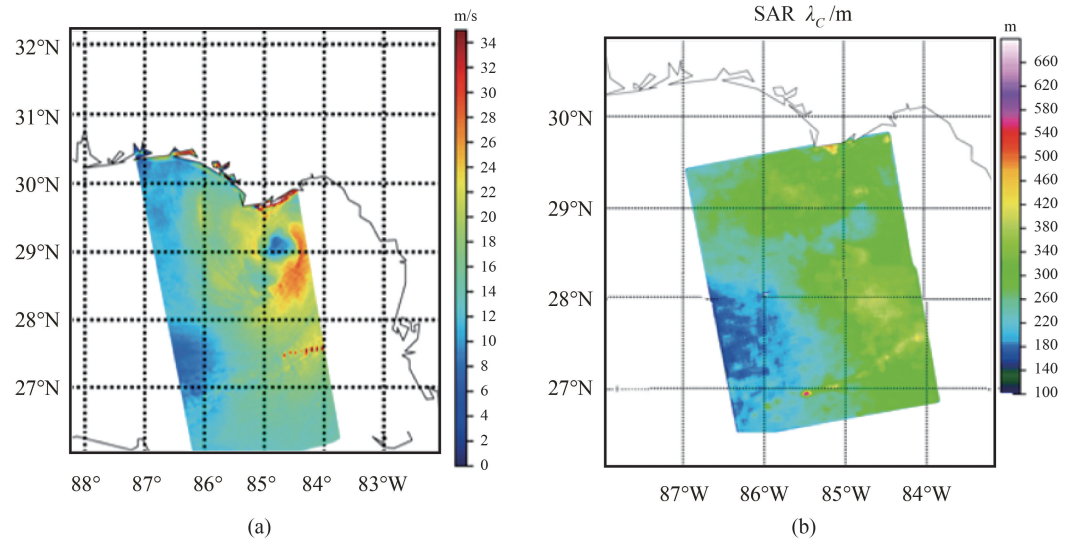

Fig.4 (a) Wind speed map provided by Ifremer for Hurricane Hermine; (b) λc map estimated taking into account the criteria described in this work for Hurricane Hermine

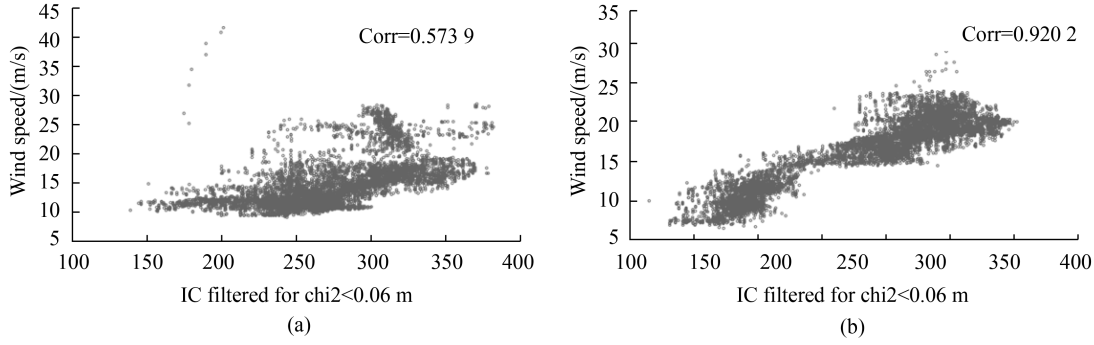

Fig.5 Scatterplot between λc values and wind speed for (a) the northern and (b) southern region of the map depicted in Fig.4

In this study, the inverse wave age factor is defined as follows[20]

$$\overline{\omega}_p = 1.2\Omega \qquad (2)$$

When $\Omega = 0.84$, and then for $\overline{\omega}_p = 1$, fully developed sea state conditions are reached. More in detail, for $\overline{\omega}_p > 1$ wind driven sea state occurs, while for $\overline{\omega}_p < 1$ mixed sea state (both wind and swell waves) occurs.

In Fig. 6 the inverse wave age factor is compared with the x^2 map for the northern area of Fig.4. One can note that there is an inverse correlation between x^2 and $\overline{\omega}_p$, since in areas dominated by lower $\overline{\omega}_p$ values are corresponding the highest x^2. Then, the x^2-approach is sorting out all those λc estimates that are under mixed sea state conditions, filtering out the box containing the swell contribute.

5 Conclusions

This study addresses the optimal choice of the azimuth cut-off estimation parameters in order to pro-

vide accurate SWH estimated under high wind conditions. The results show that:

① The median filter window size should be of about 100 mand therefore adapted to the pixel spacing.

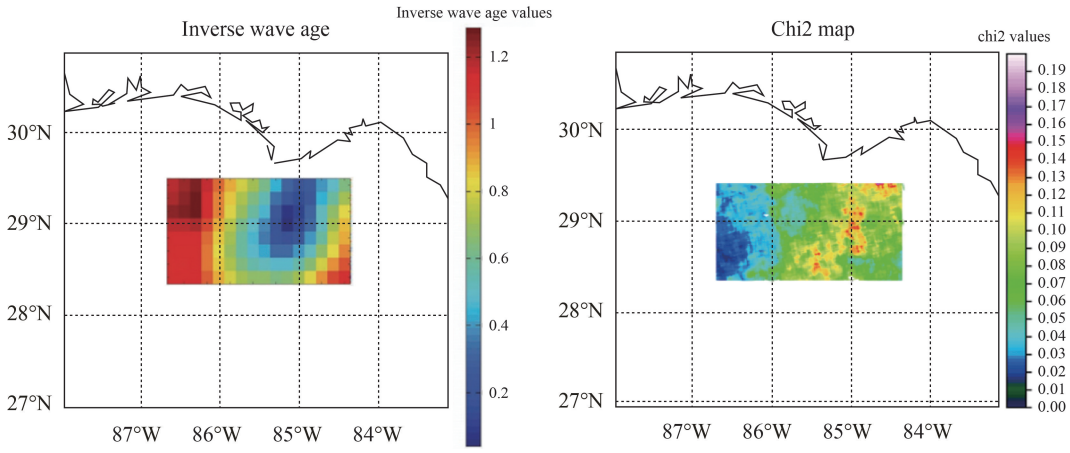

Fig.6 Inverse wave age and x^2 map for the northern area of Fig.4

② The box size should be the smallest possible since λc estimates are affected by inhomogeneities in the SAR image.

③ Unfeasible/unreliable λc values should be filtered out.

In particular, a x^2-based QC method that filters unreliable λc values is presented. By applying QC over 1-km λc estimates, the correlation between averaged 10-km λc and collocated ECMWF SWH data increases significantly.

In addition, the shown approach has been applied to a tropical cyclone showcase, and results seem to be very consistent when compared with wind speed maps provided from external sources just in some areas. In particular, an analysis carried out on the inverse wave age parameter showed that the values sorted out by the QC analysis are in correspondence with mixed sea state conditions, and, then, the more critical scenarios take place with the presence of the swell contribution.

Acknowledgements: This study was partially funded by European Space Agency (ESA) within the frame of ESA-MOST (Ministry of Science and Technology) Dragon 4 Cooperation ("Microwave satellite measurements for coastal area and extreme weather monitor", project ID 32235).

References

[1] HERSBACH H, STOFFELEN A, DE HAAN S. An improved C-band scatterometer ocean geophysical model function: CMOD5[J]. Journal of Geophysical Research: Oceans, 2007, 112(C3): C03006.

[2] LI Xiaofeng, GUO Huadong, CHEN Kunshan, et al. Advances in SAR Remote Sensing of Oceans[M]. Boca Raton: CRC Press, 2018, 1-2. DOI: 10.1201/9781351235822.

[3] DU Yanlei, YANG Xiaofeng, CHEN Kunshan, et al. An improved spectrum model for sea surface radar backscattering at L-band[J]. Remote Sensing, 2017, 9(8): 776-788. DOI: 10.3390/rs9080776.

[4] LIU Guihong, YANG Xiaofeng, LI Xiaofeng, et al. A systematic comparison of the effect of polarization ratio models on sea surface wind retrieval from C-band synthetic aperture radar [J]. IEEE Journal of Selected Topics in Applied Earth Observations and Remote Sensing, 2013, 6(3):1100-1108. DOI: 10.1109/jstars.2013.2242848.

[5] YANG Xiaofeng, LI Xiaofeng, ZHENG Quanan, et al. Comparison of ocean-surface winds retrieved from QuikSCAT scatterometer and radarsat-1 SAR in offshore waters of the U.S. west coast[J]. IEEE Geoscience and Remote Sensing Letters, 2011,8(1):163-167. DOI: 10.1109/LGRS.2010.2053345.

[6] HERSBACH H. CMOD5: an improved geophysical model function for ERS C-band scatterometry[M]//European Centre for Medium Range Weather Forecasting (ECMWF) Technical Memorandum. Shinfield Park: ECMWF, 2003, 395: 49-50.

[7] ZHOU Xuan, CHONG Jinsong, YANG Xiaofeng, et al. Ocean surface wind retrieval using SMAP L-band SAR[J]. IEEE Journal of Selected Topics in Applied Earth Observations and

Remote Sensing, 2017, 10(1): 65-74. DOI: 10.1109/JSTARS.2016.2630919.

[8] LI Xiaofeng, ZHANG Biao, and YANG Xiaofeng. Remote sensing of sea surface wind and wave from spaceborne synthetic aperture radar[J]. Journal of Radars, 2020, 9(3): 425-443. DOI: 10.12000/JR20079.

[9] KERBAOL V, CHAPRON B, VACHON P W. Analysis of ERS-1/2 synthetic aperture radar wave mode imagettes[J]. Journal of Geophysical Research: Oceans, 1998, 103(C4): 7833-7846.

[10] WANG He, ZHU Jianhua, WANG Jingsong, et al. A semiempirical algorithm for SAR wave height retrieval and its validation using Envisat ASAR wave mode data[J]. Acta Oceanologica Sinica, 2012, 31(3): 59-66.

[11] NUNZIATA F, GAMBARDELLA A, MIGLIACCIO M. An educational SAR sea surface waves simulator[J]. International Journal of Remote Sensing, 2008, 29(11): 3051-3066.

[12] GRIECO G, LIN W, MIGLIACCIO M, et al. Dependency of the sentinel-1 azimuth wavelength cut-off on significant wave height and wind speed[J]. International Journal of Remote Sensing, 2016, 37(21): 5086-5104.

[13] LI Xiaofeng, ZHANG Jun, YANG Xiaofeng, et al. Tropical cyclone morphology from spaceborne synthetic aperture radar [J]. Bulletin of the American Meteorological Society, 2013, 94(2): 215-230. DOI: 10.1175/BAMS-D-11-00211.1.

[14] ZHOU Xuan, YANG Xiaofeng, LI Ziwei, et al. Estimation of tropical cyclone parameters and wind fields from SAR images [J]. Science China Earth Sciences, 2013, 56(11): 1977-1987. DOI: 10.1007/s11430-013-4633-2.

[15] FUREVIK B R, SCHYBERG H, NOER G, et al. ASAR and ASCAT in polar low situations[J]. Journal of Atmospheric and Oceanic Technology, 2015, 32(4): 783-792. DOI: 10.1175/JTECH-D-14-00154.1.

[16] IVANOV A Y. Novaya Zemlya. Bora and polar cyclones in spaceborne SAR and optical imagery[J]. Izvestiya, Atmospheric and Oceanic Physics, 2016, 52(9): 1142-1154. DOI: 10.1134/S0001433816090127.V

[17] ZHANG Guosheng, LI Xiaofeng, PERRIE W, et al. A hurricane wind speed retrieval model for C-band RADARSAT-2 cross-polarization ScanSAR images[J]. IEEE Transactions on Geoscience and Remote Sensing, 2017, 55(8): 4766-4774. DOI: 10.1109/TGRS.2017.2699622.

[18] JIN Shaohui, LI Xiaofeng, YANG Xiaofeng, et al. Identification of tropical cyclone centers in SAR imagery based on template matching and particle swarm optimization algorithms[J]. IEEE Transactions on Geoscience and Remote Sensing, 2019, 57(1): 598-608. DOI: 10.1109/tgrs.2018.2863259.

[19] PIERSON JR W J, MOSKOWITZ L. A proposed spectral form for fully developed wind seas based on the similarity theory of S. A. Kitaigorodskii[J]. Journal of Geophysical Research Atmospheres, 1964, 69(24): 5181-5190.

[20] CHENG Yongcun, XU Qing, LIU Yuguang, et al. An analytical algorithm with a wave age factor for altimeter wind speed retrieval[J]. International Journal of Remote Sensing, 2008, 29(19): 5699-5716.